

[C II] and [N II] from dense ionized regions in the Galaxy

W. D. Langer¹, P. F. Goldsmith¹, and J. L. Pineda¹

Jet Propulsion Laboratory, California Institute of Technology, 4800 Oak Grove Drive, Pasadena, CA 91109, USA
e-mail: William.Langer@jpl.nasa.gov

Received 20 January 2016; Accepted 18 March 2016

ABSTRACT

Context. The interstellar medium (ISM) consists of highly ionized and neutral atomic, as well as molecular, components. Knowledge of their distribution is important for tracing the structure and lifecycle of the ISM.

Aims. To determine the properties of the highly ionized gas and neutral weakly ionized gas in the Galaxy traced by the fine-structure lines of ionized nitrogen, [N II], and ionized carbon, [C II].

Methods. We utilize observations of the [C II] 158 μm and [N II] 205 μm fine-structure lines taken with the high spectral resolution Heterodyne Instrument in the Far-Infrared (HIFI) on the *Herschel* Space Observatory along ten lines of sight towards the inner Galaxy to analyze the ionized ISM. The [N II] emission can be used to estimate the contribution of the highly ionized gas to the [C II] emission and separate the contributions from highly ionized and weakly ionized neutral gas.

Results. We find that [N II] has strong emission in distinct spectral features along all lines of sight associated with strong [C II] emission. The [N II] arises from moderate density extended H II regions or ionized boundary layers of clouds. Comparison of the [N II] and [C II] spectra in 31 separate kinematic features shows that many of the [C II] spectra are affected by absorption from low excitation gas associated with molecular clouds, sometimes strongly so. The apparent fraction of the [C II] associated with the [N II] gas is unrealistically large in many cases, most likely due to the reduction of [C II] by absorption. In a few cases the foreground absorption can be modeled to determine the true source intensity. In these sources we find that the foreground absorbing gas layer has C^+ column densities of order 10^{18} cm^{-2} .

Conclusions. [C II] emission arising from strong sources of [N II] emission is frequently absorbed by low excitation foreground gas complicating the interpretation of the properties of the ionized and neutral gas components that give rise to [C II] emission.

Key words. ISM: clouds — ISM: HII regions — Galaxy: center

1. Introduction

The structure and dynamics of the neutral components of the interstellar medium (ISM) are readily traced with spectrally (velocity) resolved ground based observations of H I 21-cm radiation and the rotational lines of molecular species such as CO and CS. The ionized gas can be traced by radio recombination lines and H α emission, but observations of the potentially very useful diagnostic lines of C^+ and N^+ has been difficult because their strong fine structure far-infrared emission lines, [C II] and [N II], are absorbed by the Earth's atmosphere.

Comparison of [N II] with [C II] allows one, in principle, to separate highly ionized regions (H^+ , C^+ , N^+) from neutral weakly ionized regions (H, C^+ , N) because nitrogen has a higher ionization potential (14.5 eV) than does hydrogen (13.6 eV) so that it is atomic, N, where hydrogen is atomic or molecular, and ionized, N^+ , where hydrogen is nearly completely ionized. N^+ is produced by EUV or X-ray photoionization, electron collisional ionization, or proton charge exchange (Langer et al. 2015). In contrast, carbon has an ionization potential (11.1 eV) less than that of hydrogen so C^+ arises from all regions suffused with UV. [C II] is thus produced in highly ionized regions, such as the Warm Ionized Medium (WIM), compact and extended H II regions, and dense ionized boundary layers (IBL) of clouds, as well as in neutral regions which are only weakly ionized (fractional ionization $\lesssim 10^{-2}$) such as H I clouds, PDRs, and CO-dark H_2 clouds, whereas [N II] arises only from highly ionized regions.

The COBE FIRAS survey of [C II] at 158 μm and [N II] at 122 and 205 μm in the Milky Way (Bennett et al. 1994) showed that their emission was pervasive, with [C II] the strongest far-infrared line, followed by [N II] at about one-fifth of the intensity of [C II]. COBE thus established the importance of [C II] and [N II] as diagnostic tracers of the ISM where carbon and nitrogen are ionized (Bennett et al. 1994; Fixsen et al. 1999). However, COBE had a 7° beam and velocity resolution $\sim 1000 \text{ km s}^{-1}$ and so could not provide details of the distribution of C^+ and N^+ in the Milky Way, locate the emission along the line of sight (LOS), or explore the dynamics of the gas traced by [C II] and [N II]. The Heterodyne Instrument in the Far-Infrared (HIFI, de Graauw et al. 2010) on the *Herschel* Space Observatory (Pilbratt et al. 2010) provided the first opportunity to obtain a large sample of velocity resolved [C II] and [N II] in the Galaxy in emission (Langer et al. 2010; Goldsmith et al. 2015) and absorption (Persson et al. 2014; Gerin et al. 2015). The determination of the properties of the ionized gas in emission and absorption probe higher and lower density phases of the ISM, respectively.

The *Herschel* Space Observatory Open Time Key Programme, Galactic Observations of Terahertz C^+ (GOT C+) conducted a sparse survey of velocity resolved [C II] at 157.740 μm (1900.537 GHz) along over 500 LOS throughout the disk (Langer et al. 2010; Pineda et al. 2013; Langer et al. 2014). Recently Goldsmith et al. (2015) reported on a follow up survey in [N II] of 149 LOS observed in [C II] by GOT C+. All 149 LOS were observed with PACS (Poglitsch et al. 2010) in both fine structure transitions of [N II], $^3\text{P}_2\text{--}^3\text{P}_1$ at 121.898 μm

(2459.371 GHz) and $^3\text{P}_1\text{--}^3\text{P}_0$ at $205.178\ \mu\text{m}$ (1461.134 GHz). [N II] was detected in 116 LOS at $205\ \mu\text{m}$ and in 96 of these at $122\ \mu\text{m}$, where line of sight here means the average of the 25 PACS spaxels with an effective angular resolution $\sim 47''$.

Goldsmith et al. (2015) used the two [N II] transitions observed with PACS, along with a collisional excitation model, to derive the average line of sight electron densities, $n(e)$. They found $n(e)$ were typically in the range $10 - 50\ \text{cm}^{-3}$ (although a few had larger values with a maximum of $118\ \text{cm}^{-3}$ towards the Galactic center) with an average value $29\ \text{cm}^{-3}$, much higher than densities typical of the Warm Ionized Medium. They derived N^+ column densities, $N(\text{N}^+)$, which are generally in the range $10^{16} - 2 \times 10^{17}\ \text{cm}^{-2}$, with the largest value $3.4 \times 10^{17}\ \text{cm}^{-2}$ towards the Galactic center. They suggest that these moderately high electron densities in the N^+ gas arise either in extended H II regions, IBLs around molecular clouds, or from very dense fluctuations in the WIM.

Goldsmith et al. (2015) also compared the N^+ and C^+ column densities derived from PACS [N II] and HIFI [C II] emission and found that a significant fraction, $\sim 75\%$, of the sources had more than $1/3$ of the [C II] emission arising from the dense ionized gas (see their Figure 22). Croxall et al. (2016, in preparation; J. D. Smith, private communication) found a similar result from a PACS study of [N II] and [C II] in local star-forming galaxies, namely that a significant fraction of the [C II] emission arises from the highly ionized medium.

The low spectral (velocity) resolution of PACS precludes knowing where along the line of sight the emission arises or how many components contribute to a measured intensity and thus the results are a weighted average of the emission from ionized gas in the beam. Towards the ten strongest [C II] LOS in the GOT C+ survey Goldsmith et al. (2015) observed the $205\ \mu\text{m}$ transition of N^+ with *Herschel* HIFI. [N II] was detected in all ten LOS and, together with spectrally resolved [C II], provides a more detailed look at the nature of the sources of [N II] and [C II] emission.

In this paper we analyze the conditions of the ionized gas in 31 kinematic components arising along the ten LOS observed in [N II] with HIFI. We find that the [N II] emission arises from both strong and weak [C II] components and that there is significant variation in the [C II] to [N II] ratio among components and within the line profile. Furthermore, from comparison of [N II] and [C II] spectral line shapes, we find that the [C II] in several sources is strongly absorbed by lower excitation foreground gas and many of the other sources show at least some trace of [C II] absorption. The [C II] absorption, especially in the deep absorption cases, complicates the interpretation of the physical conditions from [C II].

This paper is organized as follows. In Section 2 we present the [N II] and [C II] results. Section 3 discusses the properties of gas traced by [C II] and [N II], and Section 4 summarizes the results.

2. Results

The ten lines of sight observed in [N II] $205\ \mu\text{m}$ and [C II] $158\ \mu\text{m}$ with HIFI are listed in Table 4 of Goldsmith et al. (2015) where their column 1 gives the GOT C+ LOS label and column 2 the Galactic longitude (all sources were observed at $b = 0^\circ$). We will use the GOT C+ LOS label here which is in the form Gxxx.x+y.y where the first term gives the Galactic longitude and the second the Galactic latitude, both rounded off to one decimal place. The data reduction of [N II] and [C II] is described in Goldsmith et al. (2015) and Pineda et al. (2013), respectively,

with the exception that [C II] towards the Galactic Center, $(l, b) = (0^\circ, 0^\circ)$, was reprocessed using HIPE-13 and a different baseline matching routine used to combine observations made with two LO settings. A baseline matching routine is necessary because the spectrum towards the Galactic Center is so broad that two LO settings are required to fit the entire velocity dispersion of [C II] emission. In addition, even with two LO settings, there is only baseline over a narrow band at each end. This narrow baseline band results in some uncertainty in the baseline offset as can be seen in the slight differences in the spectrum offset here and Goldsmith et al. (2015).

The [C II] and [N II] spectra for the ten sources are shown in Figures 1 to 3. We also include the corresponding $^{13}\text{CO}(1-0)$ spectrum (Pineda et al. 2013) for four lines of sight to guide the identification of the features. The ^{13}CO spectra are sometimes useful to distinguish contributions from the different LOS components where [C II] and [N II] are strongly blended and to identify dense molecular gas associated with the [N II] and [C II] sources. The spectrum towards the Galactic Center is shown in Figure 1 and we have indicated on the figure the velocity corresponding to the local and 3 kpc arms. It can be seen that the strong [N II] feature near $-60\ \text{km s}^{-1}$ probably arises from this arm and that the [C II] emission from the Galactic center is strongly absorbed by gas likely associated with the local arm.

Several characteristics of [N II] and [C II] emission stand out in Figures 1 to 3. First, [N II] emission is generally detected wherever there is [C II], although there is significant variation in the ratio of [C II] to [N II] intensity as a function of velocity. Second, [C II] appears to be absorbed or self-absorbed in many components, and strongly so in a few sources. [C II] absorption is very clear, for example, in G316.6+0.0 and G337.0+0.0 where the peak in [N II] emission is in or very near a deep minimum in [C II] emission. In some lines of sight, such as G013.9+0.0 and G049.1+0.0, the peaks in [N II] align with a smaller dip in the [C II] emission (indicated by arrows). In other lines of sight the evidence is more suggestive than definitive, for example some [N II] peaks align with the shoulder in the [C II] emission, as in G305.1+0.0, G349.1+0.0, and G342.2+0.0 (indicated by arrows). Finally, in G305.1+0.0, G342.2+0.0, and G345.7+0.0 [N II] emission is about equal to that of [C II] in the shoulders (highlighted by ellipses). This relationship could be a result of absorption of [C II] but could also be due to a velocity shift of the N^+ gas layer with respect to the C^+ gas in the neutral PDRs. Third, most of the [N II] lines are broad (of order 10 to $20\ \text{km s}^{-1}$) compared to the velocity dispersion typical for the associated dense molecular clouds. In some of these lines the corresponding ^{13}CO spectra is composed of a couple of narrower components (see for example G316.6+0.0) so the broad [N II] and [C II] may be due to blending of a few cloud components. Fourth, ^{13}CO is not associated with the full range of [C II] emission; there are ^{13}CO spectral features with no detectable [C II] and [N II] and vice-versa. For example, in G031.3+0.0 there is strong ^{13}CO emission near $75\ \text{km s}^{-1}$ with weak [C II] and [N II], while near $100\ \text{km s}^{-1}$ the ^{13}CO is weak while [C II] and [N II] are strong. For a more detailed discussion of the relationship of [C II] and ^{13}CO emission see Pineda et al. (2013) and Langer et al. (2014).

Our goal in this paper is to understand the relative contributions of different ISM components to the [C II] intensity because of its importance in determining the Galactic [C II] distribution and its role in measuring the star formation rate (see Pineda et al. 2013, 2014). Our approach is to use the [N II] lines to calculate the expected [C II] contribution from the highly ionized gas and then subtract it from the observed [C II] to determine its contribution from the neutral gas. However, the absorption in [C II] makes

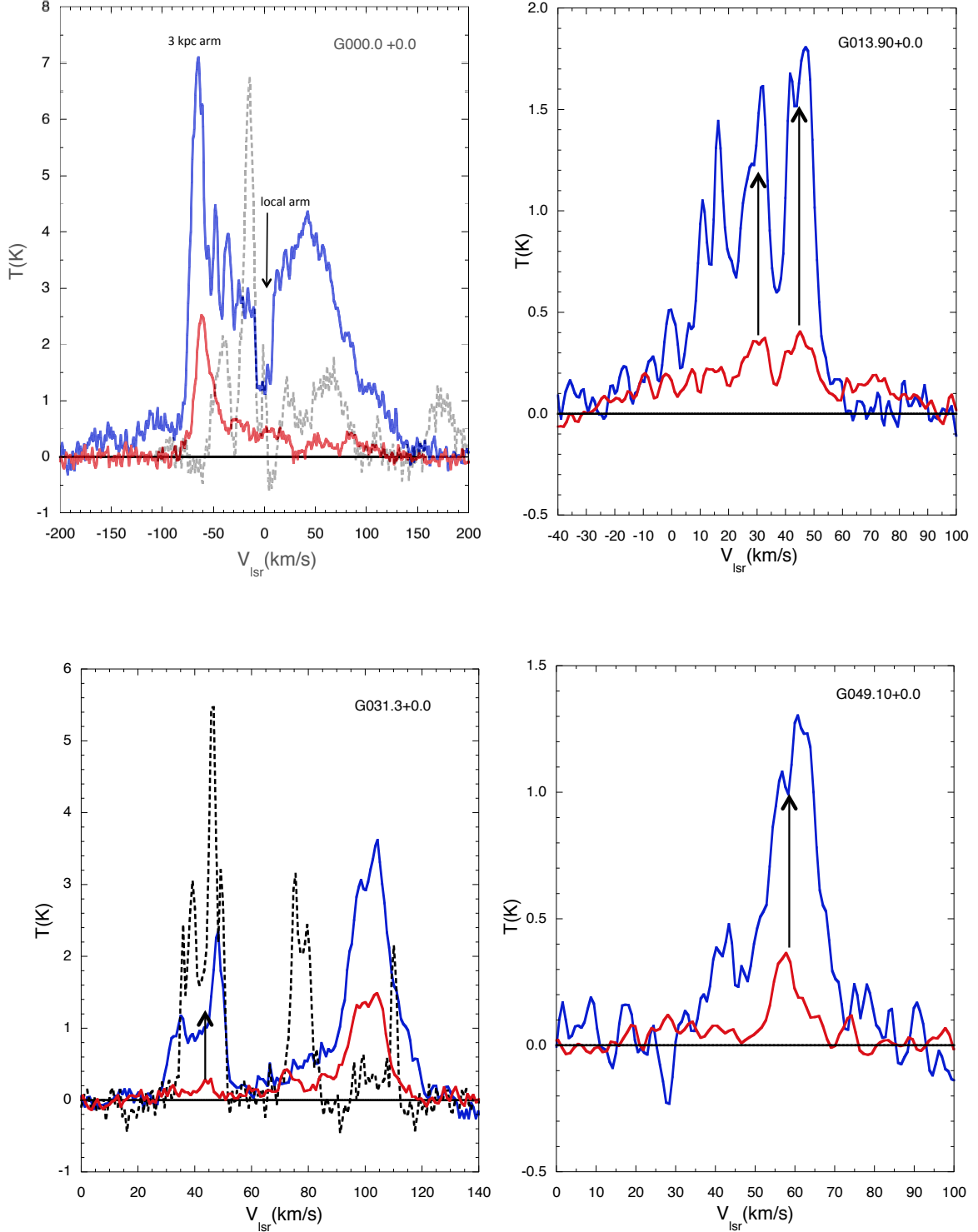


Fig. 1. Main beam temperature versus velocity for [C II] (blue solid spectra) and [N II] (red solid spectra) taken with HIFI – see Table 1 for some of the line parameters, and $^{13}\text{CO}(1-0)$ (black dashed line) from Pineda et al. (2013). Each line of sight is labeled with the GOT C+ LOS label. Some features that are indicative of [C II] absorption are highlighted with arrows.

determination of the relative contributions of [C II] from highly ionized and neutral gas problematic. In this Section we outline the procedure for calculating the [C II] contribution from ionized and neutral components neglecting absorption. In Section 3 we will address the correction for absorption.

To calculate the contribution of C^+ from the ionized N^+ region to the measured [C II] intensity we need to transform the

[N II] intensity to the expected [C II] intensity. To derive the relationship of [C II] to [N II] in a highly ionized regime we start with the formula for the relationship between intensity and column density for an optically thin species (Goldsmith et al. 2012),

$$I_{ul} = \int T_{ul} dv = \frac{hc^3}{8\pi k \nu_{ul}^2} A_{ul} N_u \quad (1)$$

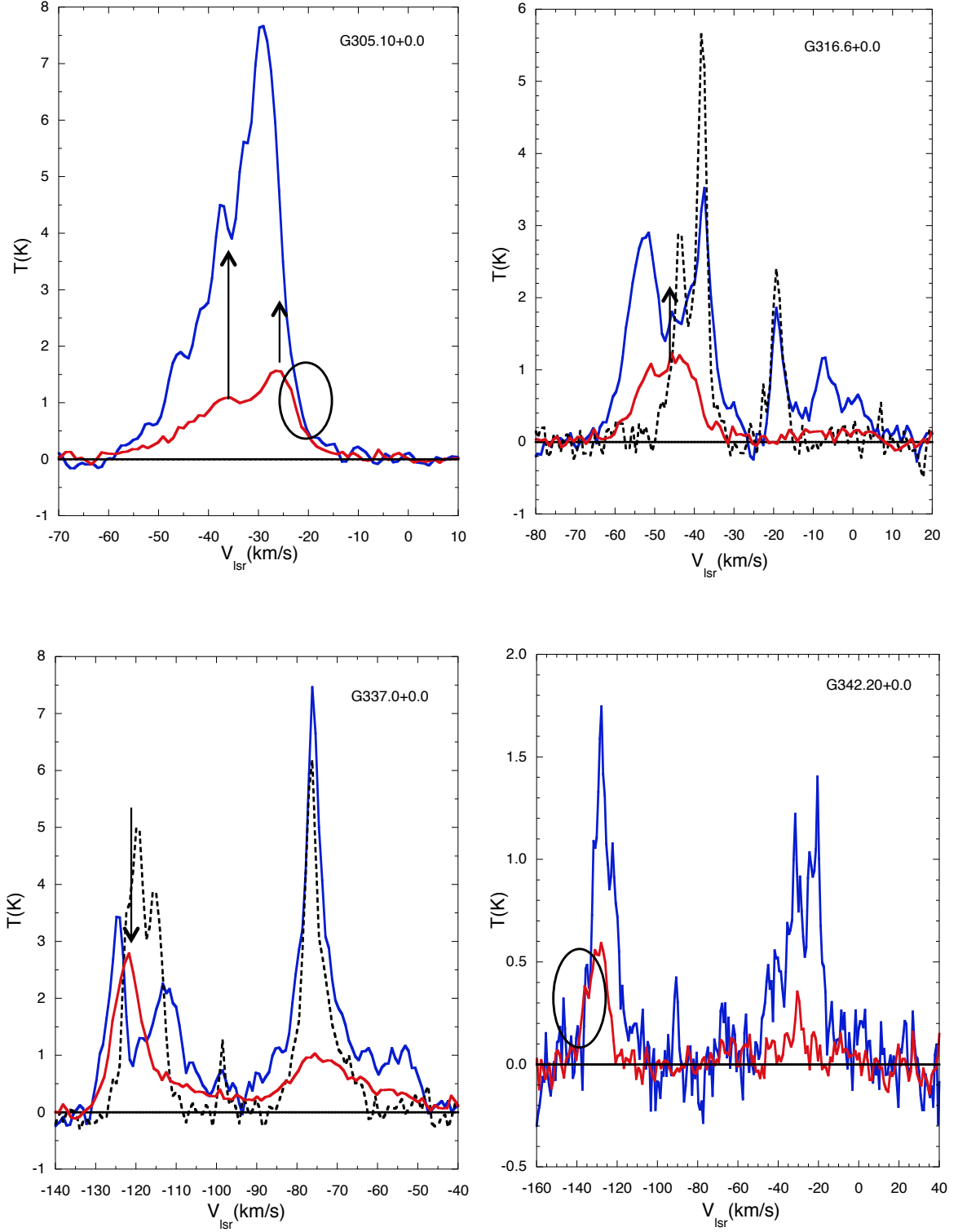


Fig. 2. Main beam temperature versus velocity for [C II] (blue solid spectra) and [N II] (red solid spectra) taken with HIFI – see Table 1 for some of the line parameters, and $^{13}\text{CO}(1-0)$ (black dashed line) from Pineda et al. (2013). Each line of sight is labeled with the GOT C+ LOS label. Some features that are indicative of [C II] absorption are highlighted with arrows and the shoulders of lines where [N II] is almost as strong as [C II] are highlighted with ellipses.

where T_{ul} is the antenna temperature of the upper (u) to lower (l) transition, ν_{ul} is the transition frequency, A_{ul} the Einstein A-coefficient, and N_u the column density of the upper level. In a uniform medium we can simplify Equation 1 by setting $N_u = f_u n(X)L$ where $n(X)$ is the density of the emitting species, X ,

L the path length of the emission region, and f_u the fractional population of the upper level, to yield,

$$I_{ul} = \int T_{ul} dv = \frac{hc^3}{8\pi k \nu_{ul}^2} A_{ul} f_u n(X) L \quad (2)$$

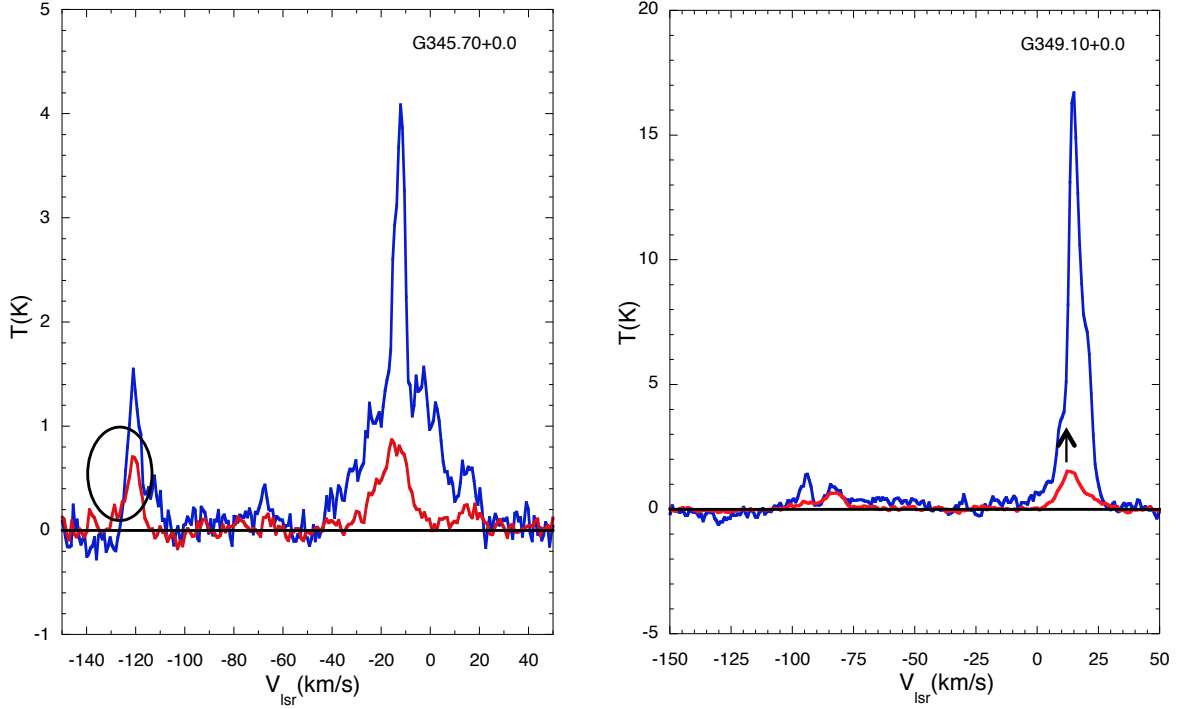


Fig. 3. Same as Figure 2.

Therefore the ratio of the [C II] 158 μm to [N II] 205 μm intensity from the N^+ gas, $I_{\text{ion}}([\text{C II}])$, in a fully ionized region, is given by

$$\frac{I_{\text{ion}}([\text{C II}])}{I_{\text{ion}}([\text{N II}])} = \frac{v_{10}^2 A_{3/2,1/2}}{v_{3/2,1/2}^2 A_{1,0}} \frac{f_{3/2} n(\text{C}^+)}{f_1 n(\text{N}^+)}, \quad (3)$$

and the contribution of [C II] emission from the N^+ region is related to the corresponding [N II] emission by

$$I_{\text{ion}}([\text{C II}]) = 0.675 \frac{f_{3/2}(\text{C}^+)}{f_1(\text{N}^+)} \frac{x(\text{C}^+)}{x(\text{N}^+)} I_{\text{ion}}([\text{N II}]), \quad (4)$$

where $x(\text{C}^+)$ and $x(\text{N}^+)$ are the fractional abundances of C^+ and N^+ , respectively, and $A_{3/2,1/2} v_{1,0}^2 / A_{1,0} v_{3/2,1/2}^2 = 0.675$. In highly ionized regions Equation 4 is a function of kinetic temperature, T_k , and $n(e)$ only through the ratio of the fractional populations of the upper levels of [C II] ($^2P_{3/2}$) and [N II] 205 μm (3P_1). We will use the values of $n(e)$ derived from PACS data (Goldsmith et al. 2015) and adopt $T_k = 8000\text{K}$, characteristic of highly ionized regions, to calculate the ratio of these fractional populations. However, the exact values of $n(e)$ and T_k are not critical because the ratio of the level populations is relatively insensitive to density and temperature as their collisional rate coefficients and critical densities, $n_{\text{cr}}(e)$, are comparable (see Goldsmith et al. 2012, 2015). For example, over the density range of interest, $n(e) = 5$ to 150 cm^{-3} , $f_{3/2}/f_1 \sim 1.38$ within $\pm 12\%$. The fractional emission derived for [C II] depends on the ratio $x(\text{C}^+)/x(\text{N}^+)$. Here we adopt the value 2.9 from Goldsmith et al. (2015), however the abundance ratio could be lower either because the elemental gas phase carbon to nitrogen ratio is smaller or ionization processes, such as photoionization near X-ray sources, could selectively change the ratio (Langer & Pineda 2015).

The total observed [C II] emission is the sum of the ionized, $I_{\text{ion}}([\text{C II}])$, and neutral, $I_{\text{neut}}([\text{C II}])$, ISM components,

$$I_{\text{tot}}([\text{C II}]) = I_{\text{ion}}([\text{C II}]) + I_{\text{neut}}([\text{C II}]), \quad (5)$$

and, in principle, the neutral component can be derived by subtracting the ionized component from the total observed [C II] emission.

We evaluate the contribution of the ionized gas to the [C II] emission for each component by determining $I([\text{N II}])$ from the HIFI spectra and solving Equation 4 using $n(e)$ from Goldsmith et al. (2015) for each LOS. For many of the [N II] spectra the components are well defined with a nearly Gaussian shape, however, some features are a blend of multiple components and for these we make an educated guess of the velocity range of the [N II] component. We have identified 31 kinematic [N II] components with $I([\text{N II}])$ signal-to-noise $\gtrsim 5$ (all corresponding [C II] components have much higher signal-to-noise). The line parameters for the 31 components analyzed here are given in Table 1, where we list in columns 1 to 9 for each LOS the velocity range of interest, the corresponding intensities of [C II] 158 μm and [N II] 205 μm , the V_{lsr} and $\Delta v([\text{N II}])$ (the full width half maximum) for [N II] and $\Delta v([\text{C II}])$ for [C II] wherever we could fit a Gaussian to the blended lines, and the average values of $n(e)$ derived by Goldsmith et al. (2015) from PACS [N II] 122 and 205 μm lines.

In general the linewidths derived for [C II] agree with those of [N II] given that it is difficult to derive an unambiguous fit for spectra with multiple blended components. In a few cases the linewidths disagree by more than a few km s^{-1} which is generally due to closely blended features where it is not possible to fit them separately. Finally, we do not derive the linewidths of [C II] lines that are significantly absorbed in the line center as the fit has little relevance for comparison to the [N II] linewidths. However, as discussed below we will use the [N II] lines in these cases to derive the likely [C II] source linewidth and intensity. In column 10 we list the derived fraction of [C II] emission that arises from the N^+ region, $I_{\text{ion}}([\text{C II}])/I_{\text{obs}}([\text{C II}])$, where $I_{\text{obs}}([\text{C II}])$ is the total observed [C II] emission. In column 11 we give this ratio for the few positions where we can correct [C II] for absorption, $I_{\text{ion}}([\text{C II}])/I_{\text{tot}}([\text{C II}])$, as will be discussed

below. In addition to the parameters for the individual spectral components, we also provide the results of integrating across the full spectrum in Table 1 for comparison to what might be expected from an instrument, such as PACS, that does not resolve the individual components.

In Figure 4 we plot the solutions for the fractional [C II] intensity arising from the N^+ region for all the individual components listed in Table 1. In addition, to simulate the solutions for the unresolved PACS [N II] spectra, we also calculated the total intensity in the HIFI [N II] and [C II] bands along each line of sight. These ten fractional intensities are plotted in Figure 5. For the Galactic Disk (blue filled circles) and Galactic center (blue filled diamonds) solutions we used the observed [C II] intensity for the total intensity, whereas the four red filled circles represent solutions for [C II] emission corrected for absorption (discussed in Section 3) and for these values we use the total corrected [C II] intensity. The ratio of $I_{\text{ion}}([\text{C II}])/I_{\text{tot}}([\text{C II}])$ must be less than one or else the fractional [C II] emission arising from the ionized gas is greater than the total observed [C II].

It can be seen that roughly one quarter of the ratios plotted in Figure 4 have $I_{\text{ion}}([\text{C II}])/I_{\text{tot}}([\text{C II}])$ greater than unity and, thus, represent an unphysical solution (before correcting for absorption). In addition a majority of the points have $I_{\text{ion}}([\text{C II}])/I_{\text{tot}}([\text{C II}])$ greater than 0.5, which while theoretically possible, is suspicious because it would indicate that the vast majority of [C II] comes primarily from the [N II] regions. However, it is more likely that the observed [C II] is not tracing all the C^+ in the ionized and neutral gas due in part to absorption of the [C II] emission. The fraction of [C II] arising from the ionized gas for the integrated line of sight emission in Figure 5 lie mainly in the range 0.5 to 0.8 in our sample of the disk, with two LOS showing values greater than one, while the Galactic center LOS has the smallest fraction. The fraction for the total LOS emission is generally less than that of the individual components, reflecting the result of averaging regions of differing physical and emission properties.

A similar result can be inferred from the PACS data in Goldsmith et al. (2015) Figure 22, where they compare the C^+ column density $N(C^+)$ from the GOT C+ data with the N^+ column density $N(N^+)$ derived from PACS. The C^+ emission that comes from the N^+ region is defined by a line corresponding to $N(C^+)=2.9N(N^+)$ on their figure. Roughly 15% of the data points fall below that line corresponding to less observed $N(C^+)$ than predicted from scaling [N II], which likely results from [C II] absorption, as seen in our HIFI data for individual spectra. Lines at $N(C^+)=2\times 2.9N(N^+)$ corresponds to half of the C^+ residing in the [N II] region. Roughly half the data points lie in the range of 50% to 100% of the C^+ associated with N^+ , which while possible, is again suspect. As discussed above, to a good approximation, the ratio of column densities is equal to that of the intensities within 10 to 20 percent for optically thin lines, so the result from PACS holds true for the fraction of [C II] emission arising from the [N II] region. Although the $N(C^+)$ to $N(N^+)$ derived from PACS may be suspect, the $n(e)$ derived by Goldsmith et al. (2015) for the average LOS should be reasonably good because they depend on the ratio of the [N II] 122 and 205 μm lines, and these lines are less likely to be affected by absorption.

In Section 3 below we show that it is possible to correct the fraction of [C II] arising from the [N II] emission region by accounting for the foreground absorption in four of the sources in which the [N II] and [C II] line shapes allow us to estimate the source intensity and correct for absorption. The foreground absorption is significant and results in at least a 40% reduction in the observed [C II] arising from the dense ionized regions.

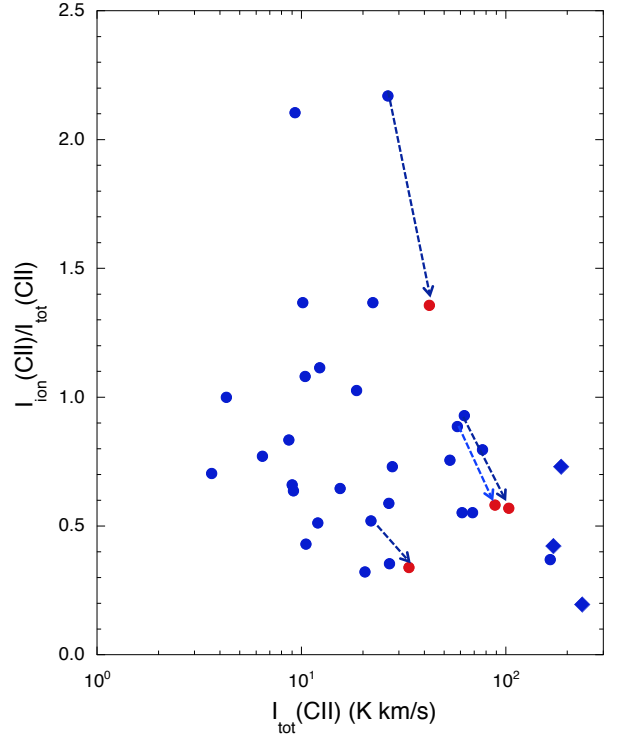


Fig. 4. [C II] intensity in the ionized gas, $I_{\text{ion}}([\text{C II}])$, calculated from the observed [N II] intensity, as a fraction of the total [C II] intensity, $I_{\text{tot}}([\text{C II}])$, versus the total [C II] intensity for thirty one [N II] components (28 Galactic Disk and 3 Galactic center). The blue filled circles and blue filled diamonds are Galactic Disk and Galactic center sources, respectively. $I_{\text{tot}}([\text{C II}])$ equals the observed [C II] intensity, $I_{\text{obs}}([\text{C II}])$ (uncorrected for [C II] foreground absorption). The four sources which are corrected for foreground absorption are shown by the red filled circles, where the total [C II] intensity, $I_{\text{tot}}([\text{C II}])$, is the corrected value to the observed intensity. The dashed blue arrows connect the corresponding uncorrected and corrected solutions. A ratio greater than 1.0 corresponds to a prediction of [C II] arising from the [N II] region greater than that observed.

3. Discussion

The results presented in Section 2 show that the observed [C II] in many kinematic components is probably not tracing all the material in which it originates. The most likely scenario to explain the absorption suggested by the spectra in Figures 1 to 3 is that emission of [C II] from a high excitation region on the far side of a cloud is absorbed by low excitation [C II] on the near side, or by a few clouds along the line of sight, or for the inner Galaxy, where there is near- far-distance ambiguity, that emission from a distant spiral arm is absorbed by the near spiral arm at the same velocity. The absorbing gas must have an excitation temperature considerably lower than that of the emission region. In addition to the absorption seen in [C II] by comparison with the [N II] spectra shown here, absorption of [C II] and [N II] has also been seen in several sources against bright star forming regions (Gerin et al. 2015; Persson et al. 2014) and is attributed to the warm ionized medium for [N II] and, mainly, to the cold neutral medium for [C II]. Absorption in [C II] has also been inferred in very bright H II regions from comparison of [C II] with its weaker isotopologue $[^{13}\text{C II}]$ (Graf et al. 2012; Ossenkopf et al. 2013; Stutzki et al. 2013). As discussed above, other factors that

Table 1. [N II] and [C II] Kinematic Features and Line Properties

LOS label	#	V range (km s ⁻¹)	$I([\text{C II}])^a$ (K km s ⁻¹)	$I([\text{N II}])^a$ (K km s ⁻¹)	$V_{lsr}([\text{N II}])^b$ (km s ⁻¹)	$\Delta v([\text{N II}])^b$ (km s ⁻¹)	$\Delta v([\text{C II}])^b$ (km s ⁻¹)	$n(e)^c$ (cm ⁻³)	$I_{ion}([\text{C II}]) / I_{obs}([\text{C II}])$ observed	$I_{ion}([\text{C II}]) / I_{tot}([\text{C II}])$ $\tau_{corrected}^d$
G000.0+0	1	-90→-35	186.8	54.0	-60.3	16.8	18.7	118	0.73	-
	2	-35→30	171.0	28.6	-	-	-	118	0.42	-
	3	30→140	236.6	18.3	-	-	-	118	0.20	-
	total	-200 → 200	629.1	97.9	-	-	-	118	0.39	-
G013.9+0	1	-5→5	4.3	1.7	-	-	-	27	1.00	-
	2	5→15	9.1	2.4	-	-	-	27	0.64	-
	3	15→25	12.0	2.5	30.4	15.9	12.9	27	0.51	-
	4	25→35	15.5	4.1	45.1	14.4	11.3	27	0.64	-
	5	35→60	26.8	6.4	-	-	-	27	0.59	-
	total	-50 → 60	68.3	17.4	-	-	-	27	0.63	-
G031.3+0	1	25→60	27.0	3.9	-	-	-	31	0.35	-
	2	60→85	10.2	5.7	-	-	-	31	1.37	-
	3	85→120	62.7	23.9	100.8	15.5	18.4	31	0.93	0.57
	total	0→130	100.7	32.8	-	-	-	31	0.80	-
G049.1+0	1	30→45	3.6	1.0	-	-	-	20	0.74	-
	2	45→75	21.9	4.5	57.9	8.7	14.2 ^e	20	0.55	0.34
	total	0 → 90	26.2	5.8	-	-	-	20	0.57	-
G305.1+0	1	-60→-40	27.8	8.5	-45.5	10.8 ^f	-	56	0.82	-
	2	-40→-30	61.0	14.1	-36.6	8.3 ^f	-	56	0.62	-
	3	-30→-10	53.2	16.8	-26.5	8.8 ^f	-	56	0.84	-
	total	-80 → 0	131.2	37.3	-	-	-	56	0.68	-
G316.6+0	1	-70→-25	58.0	20.5	-46.5	16.4	-	23	0.94	0.58
	2	-25→15	20.5	2.6	-	-	-	23	0.34	-
	total	-80 → 20	78.4	23.4	-	-	-	23	0.75	-
G337.0+0	1	-135→-115	26.5	23.5	-121.8	9.3	-	30	2.37	1.36
	2	-115→-95	18.6	7.8	-	-	-	30	1.12	-
	3	-95→-40	76.9	25.0	-73.7	20.5 ^e	7.3	30	0.87	-
	total	-140 → -40	121.9	56.7	-	-	-	30	1.14	-
G342.2+0	1	-150→-110	22.3	11.5	-129.9	13.0	12.5	14	1.37	-
	2	-50→-35	6.5	1.9	-	-	-	14	0.77	-
	3	-35→-26	8.7	2.7	-	-	-	14	0.84	-
	4	-26→-10	10.5	1.7	-	-	-	14	0.43	-
	total	-150 → -40	48.5	23.1	-	-	-	14	1.27	-
G345.7+0	1	-130→-100	12.3	5.7	-121.0	6.9	6.5	60	1.24	-
	2	-50→5	68.8	15.9	-14.9	14.7 ^e	9.0	60	0.62	-
	3	5→25	9.0	2.5	-	-	-	60	0.74	-
	total	-130 → 25	95.4	23.10	-	-	-	60	0.58	-
G349.1+0	1	-110→-88	10.4	4.7	-83.1	9.4	7.7	66	1.20	-
	2	-88→-75	9.3	8.2	-	-	-	66	2.33	-
	3	-5→35	164.9	25.4	13.7	10.7	8.6	66	0.41	-
	total	-110 → 35	201.6	42.3	-	-	-	66	0.51	-

a) The intensities in this table are derived over a velocity range either judged by eye, or fixed using a Gaussian wherever [N II] spectra could be fit unambiguously, in which case we also list their V_{lsr} and Δv . The second column numbers the individual components in order of appearance in the band from low to high velocity. Most values are rounded off to one decimal place. (b) V_{lsr} and Δv from a Gaussian fit. (c) Derived by Goldsmith et al. (2015) from PACS [N II] 205 μm and 122 μm data. (d) See Section 3 and Table 2 for correction for absorption. (e) Blend of two closely spaced lines broadens the fit. (f) Multigaussian fit to three overlapping lines with distinct local maxima.

could affect the fractional emission derived for [C II] are optically thick [C II] lines and the adopted value of the ratio of C^+ to N^+ . If the ratio $x(\text{C}^+)/x(\text{N}^+)$ is smaller than the value adopted in Section 2, for example if the elemental gas phase carbon to nitrogen ratio is lower, then the intensity $I_{ion}([\text{C II}])$ will be smaller.

3.1. Spectral line absorption

Absorption of [C II] and [N II] by a low excitation envelope or by foreground gas (both local or in a near-distance spiral arm) will be different for N^+ and C^+ because each of these species occupy different volumes along the line of sight. C^+ will be found in highly ionized regions (the warm ionized medium) and in neutral regions (the warm neutral medium, H I clouds, and CO-dark H₂ regions), but N^+ is present essentially only in the warm ion-

ized medium, H II regions, and IBLs. Furthermore, in the highly ionized regions N^+ will be less absorbed than C^+ because it has a lower column density due to its lower fractional abundance relative to C^+ (here $x(\text{C}^+)/x(\text{N}^+) \sim 2.9$). Finally, we might expect different degrees of absorption due to the geometry of the gas and the requirement that absorption occurs mainly from gas that is within the velocity range of the emission region.

Along the ten lines of sight observed with HIFI the electron densities derived by Goldsmith et al. (2015) (see Table 1) are high enough to readily excite the upper fine-structure levels of N^+ and produce the strong [N II] emission observed with HIFI. For $n(e) \sim 20 - 50 \text{ cm}^{-3}$ the excitation temperature for the [N II] in the ionized gas is high, $\sim 40 - 50 \text{ K}$, and similarly for [C II]. The N^+ column densities derived by Goldsmith et al. (2015) range from 3 to $19 \times 10^{16} \text{ cm}^{-2}$ for the Disk, with an av-

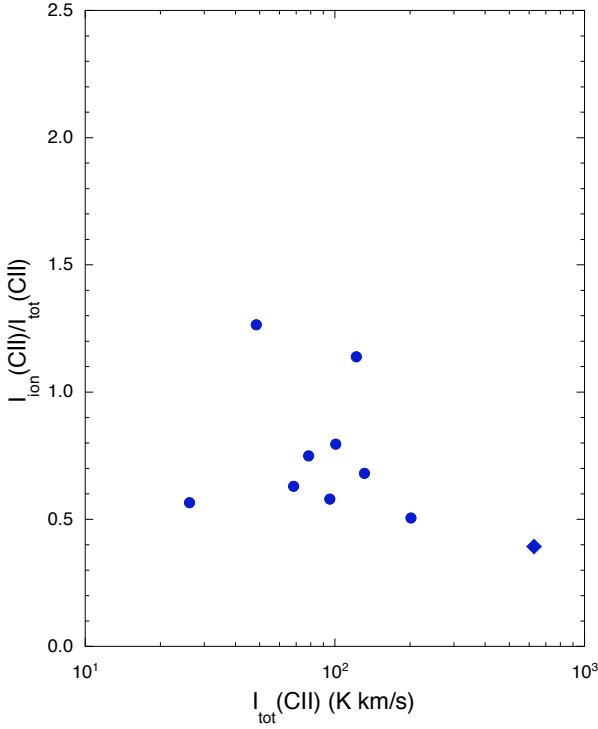


Fig. 5. Same as Figure 4 but calculated for the total emission within the [C II] and [N II] bands along each of ten lines of sight as it would be observed by a low resolution spectrometer. The blue filled circles and blue filled diamond are the Galactic Disk sources and the Galactic center source, respectively, where $I_{tot}([C II])$ equals the observed [C II] intensity, $I_{obs}([C II])$, uncorrected for foreground absorption. A ratio greater than 1.0 corresponds to a predicted [C II] arising from the [N II] region greater than that observed.

erage value $\sim 10^{17} \text{ cm}^{-2}$, and $3.4 \times 10^{17} \text{ cm}^{-2}$ for the Galactic center. We cannot know from the PACS data the actual electron densities of each velocity component or range, but it seems a reasonable starting point to adopt a characteristic density for the brightest [N II] components derived from PACS. The column density derived from PACS is a total column density along the line of sight and the individual component column densities will be smaller where there are multiple components of comparable intensity, as seen in Figures 1 to 3 for G013.9+0.0, G031.3+0.0, G305.1+0.0, G337.0+0.0, and G345.7+0.0.

3.1.1. [N II] opacity

To determine the potential effect of absorption on the [N II] spectral lines we first estimate the maximum opacity for the ground state transition in the emission region using the density and column density solutions from Goldsmith et al. (2015). The opacity of the $^3P_1 - ^3P_0$ transition for [N II] is given by (Persson et al. 2014; Goldsmith et al. 2015)

$$\begin{aligned} \tau_{10}(N^+) &= \frac{g_1 A_{10} c^3 N_0(N^+)}{g_0 8 \pi \nu_{10}^3 10^5 \Delta \nu} \\ &= 2.1 \times 10^{-17} \frac{N_0(N^+)}{\Delta \nu} \text{ cm}^{-2}, \end{aligned}$$

where $\Delta \nu$ is the linewidth in km s^{-1} and $N_0(N^+)$ is the column density of N^+ in the 3P_0 state in cm^{-2} . The fractional popula-

tion in the 3P_0 state is ~ 0.5 for the electron densities derived for the [N II] emission region. For a typical column density $N(N^+) \sim 10^{17} \text{ cm}^{-2}$ and [N II] linewidth of $\sim 10 \text{ km s}^{-1}$, $N_0(N^+) \sim 5 \times 10^{16} \text{ cm}^{-2}$ and $\tau_{10}(N^+) < 0.1$. As the total column densities for N^+ in the emission region (Goldsmith et al. 2015) are less than $2 \times 10^{17} \text{ cm}^{-2}$ in the Disk and $3.4 \times 10^{17} \text{ cm}^{-2}$ towards the center, the [N II] opacity in the emission region is small and self-absorption in [N II] is negligible. In the foreground absorption region, where the densities are lower, the fractional population in the ground state is ~ 1 and it would take a column density $N(N^+) \gtrsim 5 \times 10^{17} \text{ cm}^{-2}$ to have any significant absorption.

There are three possible sources of [N II] absorption, the extended WIM along the line of sight, a lower density portion of the extended H II region, and the ionized boundary layer along the front side of the cloud or near-distance spiral arm. Persson et al. (2014) detected only two [N II] sources in absorption with a ground state column density of absorbing $N^+ \sim 1.5 \times 10^{17} \text{ cm}^{-2}$ and attributed it to the extended WIM. They estimated the WIM gas density to be $n(H^+) \sim 0.1 \text{ cm}^{-3}$. The absorption detected by Persson et al. (2014) occurs over kpc scales and velocity dispersion $\sim 40 - 50 \text{ km s}^{-1}$ much larger than that of [N II] in emission observed in our sources. Thus absorption by low density WIM is unlikely to be significant in our HIFI sources due to the lack of a large column density for $N_0(N^+)$ within the velocity range of [N II] emission features. If absorption is due to the dense ionized boundary layer on the front side of the cloud then the total column density $N(N^+)$ derived by Goldsmith et al. (2015) for disk sources corresponds to $\tau(N^+) \lesssim 0.2$ and even smaller in the case of multiple components along the line of sight. Therefore [N II] is only slightly absorbed by gas local to the emission region and this result is consistent with the low level of absorption seen in the [N II] spectra in Figures 1 to 3.

3.1.2. [C II] absorption

Whereas there is no, or at most very little, absorption seen in the [N II] spectra, there is significant to moderate absorption of [C II] in most of the ten LOS. If we can calculate the [C II] intensity and line shape of the source we can determine the true contributions of [C II] in the ionized and neutral gas, as well as determine the opacity of the absorbing layer. However, determining the properties of the absorbing material and its column density is difficult in most cases because the [C II] profiles are either too complex or too blended to generate a unique solution to the emission source line.

There are four lines of sight for which it is possible to estimate the profile and strength of the [C II] source by fitting the intensity as a function of velocity in the [C II] line wings with a Gaussian, using information from the corresponding [N II] spectra as constraints on the [C II] solution. To estimate the true [C II] emission line profile that would be observed in the absence of absorption we fit a Gaussian to the wings of the [C II] line, adopting a two step process. First we scale the peak $T_{mb}(K)$ of the Gaussian fit to [N II] fixing V_{lsr} and $\Delta \nu$ until the line wings match those of [C II] as well as possible, where the line wings are defined as the regions outside of the FWHM. This procedure assumes that the line profiles of the [C II] and [N II] can be represented by similar Gaussians (having comparable V_{lsr} and $\Delta \nu$), which should be an adequate first approximation because we find comparable linewidths for [C II] and [N II] in those cases where the lines can be fit unambiguously, as seen in Table 1. We then refine the Gaussian fit to the [C II] line wings adjusting the peak temperature, V_{lsr} , and $\Delta \nu$ until we minimized the

difference across the observed line wings. In Figure 6 we show the Gaussian fit representing the source, along with the observed [C II] and [N II] spectra, for one LOS, G316.6+0.0. In Table 2 we list the peak source antenna temperature, T_s and integrated intensity, $I_{tot}([C II])$, of the Gaussian fit to the [C II] line wings for the four sources.

We then recalculate the fraction of [C II] that arises from the [N II] region using the revised total intensity ($I_{tot}([C II]) > I_{obs}([C II])$) and the values are given in Table 2 along with the uncorrected value from Table 1. Comparison of the fitted [C II] emission with that expected from the region producing [N II] emission reduces the fraction of [C II] from the ionized region by about 40% in the four sources. The revised values for the fractional [C II] arising from the ionized regions for these four sources is also plotted separately in Figure 4 as red filled circles, an arrow connects the values before and after correction for absorption. It can be seen that three of the four corrected sources have the fractional contributions to [C II] from the [N II] region reduced to ≤ 0.6 , but that the source with the highest ratio still has a fraction greater than unity. There are two possible explanations, either we have underestimated the absorption and/or the [C II] lines are optically thick and need to be corrected for it.

3.1.3. Foreground opacity

Assuming the Gaussian fits to [N II] and the line wings of [C II] in Section 3.1.2 are correct we can calculate the [C II] foreground opacity from the projected [C II] source intensity, $I_{tot}([C II])$, and the observed [C II] intensity, $I_{obs}([C II])$, as a function of velocity. At line center we define the opacity in terms of the reduction in the peak intensity, $\tau_0 = \ln(T_s/T_o)$, where T_s is the corrected peak main beam temperature of the source, and T_o is the observed main beam temperature at V_{lsr} . We neglect [C II] re-emission from the foreground absorbing gas as it is likely to be small at low excitation temperatures. If there were re-emission then τ_0 would be underestimated. In Table 2 we list T_s and T_o for each LOS component along with the V_{lsr} and Δv of the absorption. The peak foreground opacity τ_o is given in column 1. The column density of the foreground C^+ in the low excitation limit is (Eq. (35), Goldsmith et al. 2012),

$$N(C^+) = 1.3 \times 10^{17} \tau(C^+) \Delta v \text{ cm}^{-2} \quad (6)$$

where Δv is in km s^{-1} .

We find that $N(C^+)$ ranges from 0.9 to $1.6 \times 10^{18} \text{ cm}^{-2}$. The opacity of the absorbing layer in G316.6+0.0 and G337.0+0.0, $\tau_0 \sim 1.3$ to 1.5, are the largest of the four sources. The absorption in these strong sources is consistent with the deep self-absorption in other [C II] sources derived from comparison of hyperfine lines of $^{13}\text{C II}$ with [C II] in a number of bright [C II] sources such as NGC2024 (Graf et al. 2012; Stutzki et al. 2013) and MonR2 (Ossenkopf et al. 2013), and a suggestion of absorption in NGC 3603, Carina North, and NGC 7023 (Ossenkopf et al. 2013). This comparison is consistent with the [C II] and [N II] emission in G316.6+0.0 and G337.0+0.0 arising from bright extended H II sources. The remaining two sources G031.3+0.0 and G049.1+0.0 are weaker [C II] sources and the corresponding absorbing layers have a lower peak optical depth $\tau_0 \sim 0.8$.

To compare the thickness of the C^+ absorbing layer with models we need to convert $N(C^+)$ to visual extinction, $A_V(\text{mag})$. We assume that the absorbing layer is located in a low density H_2 envelope. We adopt a fractional abundance $x(C^+)$ with respect to H_2 of 6×10^{-4} appropriate to the inner Galaxy, $R_{gal} \sim 3 -$

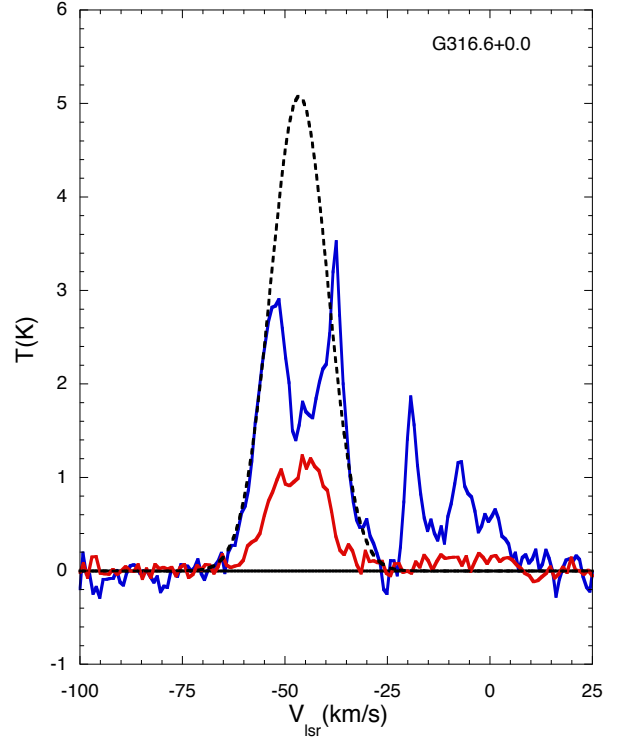


Fig. 6. A Gaussian fit (black dash) to the line wings of the $V_{lsr} \sim -47 \text{ km s}^{-1}$ [C II] component (blue) in G316.6+0.0 using the V_{lsr} and line width of the Gaussian fit (not shown) to the [N II] emission (red).

4 kpc (Pineda et al. 2013), where the [C II] and [N II] sources are likely located, and the values of A_V are included in the last column of Table 2. The estimated thickness of the absorbing layer in the components in two of the [C II] sources, G049.1+0.0 and G337.0+0.0, is comparable to those predicted by PDR models of clouds (Visser et al. 2009; Glover et al. 2010; Wolfire et al. 2010; Glover & Mac Low 2011) in which the atomic hydrogen plus CO-dark H_2 layer has $A_V \sim 1 \text{ mag}$, roughly independent of cloud mass, density, and radiation field. Thus absorption in these two [C II] sources can probably be explained with standard models of the layer of low density atomic and molecular gas layers. However, two sources, G031.3+0.0 and G316.6+0.0, have absorbing layers with column densities or extinctions much larger than predicted by the standard PDR models. One simple explanation could be that a couple of clouds at comparable velocities located in proximity to each other combine to produce the total line of sight absorption. The bright [C II] sources in these ten lines of sight occur in the dense spiral arms where such crowding is likely. For inner Galaxy sources another possibility is that emission from a distant spiral arm is absorbed by clouds in a near-distance spiral arm at the same velocity.

3.2. Carbon to nitrogen abundance

In addition to absorption of [C II] emission by low excitation foreground gas the amount of [C II] calculated to arise from the N^+ region using the [N II] as a tracer depends on the C^+ to N^+ ratio. It can be smaller than the value adopted from Goldsmith et al. (2015), either due to differences in elemental abundances or to atomic processes that alter the ratio of $x(C^+)/x(N^+)$ (Langer & Pineda 2015). For example, enhanced

Table 2. [C II] emission and absorption components

[C II] Source Component						[C II] Absorber Component					
LOS label	#	T_s (K)	$I_{tot}(\tau)$ (K km s ⁻¹)	I_{ion}/I_{obs} observed	I_{ion}/I_{tot} corrected	T_o (K)	V_{lsr} (km s ⁻¹)	Δv (km s ⁻¹)	τ_0	$N(C^+)$ 10 ¹⁸ cm ⁻²	A_v mag.
G031.3	3	6.3	103.5	0.93	0.56	2.9	101	14.5	0.76	1.6	2.9
G049.1	2	3.7	33.6	0.55	0.34	1.5	59	6.7	0.89	0.9	1.6
G316.6	1	5.1	88.5	0.94	0.58	1.4	-47	8.3	1.3	1.5	2.8
G337.0	1	4.3	42.3	2.37	1.37	1.0	-121	4.5	1.5	0.9	1.7

ionization by X-rays of C^+ to high ionization states (C^{++} , etc.) relative to N^+ multiple ionization (N^{++} , etc.), will create a deficit in C^+ compared to N^+ . Multiply ionized states of C, N, and O are predicted in models of H II –PDR regions in the ionized boundary layers of clouds (Abel et al. 2005) and in models incorporating large X-ray fluxes (Langer & Pineda 2015). In addition, the fine-structure lines of [N III] at 57.3 μ m and [O III] at 88.4 and 57.4 μ m, respectively, have been observed in H II regions, as well as Helium recombination lines, so some process is available to produce highly ionized carbon and nitrogen. Unfortunately, [C III] and [C IV] do not have fine-structure transitions, so we do not have a direct way to measure the multiple ionization of C^+ . For enhanced ionization of C^+ relative to N^+ to explain some (or most) of the increased [N II] to [C II] ratio, there must be a selective process that preferentially ionizes C^+ more efficiently than N^+ and/or a significant difference in recombination rates. Thermal ionization by electrons can also enhance the loss of C^+ with respect to N^+ because of the different ionization potentials of carbon and nitrogen, but it requires high temperatures ($> 40,000$ K). X-rays or extreme ultraviolet (EUV) photoionization are possible explanations, however it will depend on the details of the relative cross sections, ionization rates, recombination rates, and gas temperatures. Such detailed modeling is beyond the scope of this paper.

4. Summary

To study the relative contribution of ionized and neutral regions of the ISM to the observed [C II] emission we identified 31 kinematic [N II] components with high signal to noise (≥ 5) along ten lines of sight in the Galactic plane using spectrally resolved [C II] (158 μ m) emission from the GOT C+ survey (Langer et al. 2010; Pineda et al. 2013) and spectrally resolved [N II] (205 μ m) from Goldsmith et al. (2015), both obtained with *Herschel* HIFI. We used the [N II] spectra to estimate how much [C II] emission arises from the highly ionized gas and derive how much from the neutral gas containing only C^+ and atomic nitrogen, N^o . Comparison of [N II] and [C II] show three important characteristics: 1) the ratio of [C II] to [N II] varies significantly from source to source and across the spectra, 2) the [N II] and [C II] lines are broad compared to those, such as ¹³CO, from the shielded regions of dense molecular clouds, and, 3) many of the [C II] lines are absorbed, sometimes strongly so, by foreground material and do not reflect the intrinsic source luminosity.

The [C II] and [N II] intensities are used to separate the amount of [C II] arising from highly ionized gas versus that which arises from C^+ in the largely neutral gas. However in a large number of components the results were unphysical, in that the [C II] calculated to be produced by the [N II] region was relatively large and, in some cases, exceeded the observed [C II] intensity. Examination of the [C II] and [N II] spectra in Figures 1 to 3 show that many [C II] spectra appear to be absorbed and

some strongly absorbed. This absorption is likely responsible for some, if not all, of the modified observed ratio because the intrinsic [C II] source intensity will be larger than observed and thus the ratio of [C II] from the ionized gas (estimated from [N II]) to the total [C II] will be reduced. In four sources we were able to calculate the effects of absorption on the [C II] intrinsic intensity and showed that, by correcting for the foreground opacity, the fraction of [C II] arising from the ionized gas with respect to the total [C II] intensity is reduced by about 40%. Three of these four sources resulted in fractional contributions from the [N II] region, $I_{ion}([C II])/I_{tot}([C II])$ about 35 to 60 percent, however one source was only reduced to 137 percent, which is unphysical.

In summary our observations of spectrally resolved [C II] and [N II], taken at face value, indicate that the contribution of [C II] from [N II] regions is large. However, there is evidence that [C II] spectra suffer from significant absorption and that one must be cautious in using [C II] from ionized regions because of absorption of [C II] by local foreground material or a foreground spiral arm. We showed that it is possible in some cases to estimate the [C II] absorption and calculate the intrinsic [C II] source intensity. However, even with these corrections the fraction of [C II] arising from [N II] regions is large, raising the possibility that high density ionized gas is responsible for significant fraction of [C II] emission. Other factors that could change the interpretation of the fraction of [C II] that arises from [N II] gas include: 1) if the [C II] lines are optically thick, and 2) if the fractional abundance ratio of C^+ to N^+ is different than assumed here, due either to an intrinsic difference in abundance or ionization processes that preferentially ionizes C^+ with respect to N^+ .

Our analysis of the fractional contribution of [C II] from [N II] regions using spectrally resolved HIFI spectra are consistent with the PACS [N II] results showing that over 50% of the lines of sight have large contributions of the ionized gas to the observed [C II]. One must be especially careful in interpreting the properties of ionized and neutral regions with spectrally unresolved, or poorly resolved, [N II] and [C II] spectra, because the effects of [C II] absorption can be large. Finally, we note that the ten lines of sight observed with HIFI are among the strongest [C II] sources in the GOT C+ survey, so we need further high spectral resolution observations of [N II] and [C II] from weaker sources to understand whether significant amounts of [C II] arise from highly ionized regions along such lines of sight, and whether absorption is important in these regions too.

Acknowledgements. We thank Dr. T. Velusamy for providing the Galactic center [C II] spectrum and for critical comments. We also thank an anonymous referee for comments and suggestions that improved the discussion. This work was performed at the Jet Propulsion Laboratory, California Institute of Technology, under contract with the National Aeronautics and Space Administration.

References

- Abel, N. P., Ferland, G. J., Shaw, G., & van Hoof, P. A. M. 2005, *ApJS*, 161, 65
Bennett, C. L., Fixsen, D. J., Hinshaw, G., et al. 1994, *ApJ*, 434, 587

- de Graauw, T., Helmich, F. P., Phillips, T. G., et al. 2010, *A&A*, 518, L6
- Fixsen, D. J., Bennett, C. L., & Mather, J. C. 1999, *ApJ*, 526, 207
- Gerin, M., Ruaud, M., Goicoechea, J. R., et al. 2015, *A&A*, 573, A30
- Glover, S. C. O., Federrath, C., Mac Low, M.-M., & Klessen, R. S. 2010, *MNRAS*, 404, 2
- Glover, S. C. O. & Mac Low, M.-M. 2011, *MNRAS*, 412, 337
- Goldsmith, P. F., Langer, W. D., Pineda, J. L., & Velusamy, T. 2012, *ApJS*, 203, 13
- Goldsmith, P. F., Yıldız, U. A., Langer, W. D., & Pineda, J. L. 2015, *ApJ*, 814, 133
- Graf, U. U., Simon, R., Stutzki, J., et al. 2012, *A&A*, 542, L16
- Langer, W. D., Goldsmith, P. F., Pineda, J. L., et al. 2015, *A&A*, 576, A1
- Langer, W. D. & Pineda, J. L. 2015, *A&A*, 580, A5
- Langer, W. D., Velusamy, T., Pineda, J. L., et al. 2010, *A&A*, 521, L17
- Langer, W. D., Velusamy, T., Pineda, J. L., Willacy, K., & Goldsmith, P. F. 2014, *A&A*, 561, A122
- Ossenkopf, V., Röllig, M., Neufeld, D. A., et al. 2013, *A&A*, 550, A57
- Persson, C. M., Gerin, M., Mookerjee, B., et al. 2014, *A&A*, 568, A37
- Pilbratt, G. L., Riedinger, J. R., Passvogel, T., et al. 2010, *A&A*, 518, L1
- Pineda, J. L., Langer, W. D., & Goldsmith, P. F. 2014, *A&A*, 570, A121
- Pineda, J. L., Langer, W. D., Velusamy, T., & Goldsmith, P. F. 2013, *A&A*, 554, A103
- Poglitsch, A., Waelkens, C., Geis, N., et al. 2010, *A&A*, 518, L2
- Stutzki, J., Graf, U. U., Simon, R., et al. 2013, in *IAU Symposium*, Vol. 292, *IAU Symposium*, ed. T. Wong & J. Ott, 57–58
- Visser, R., van Dishoeck, E. F., & Black, J. H. 2009, *A&A*, 503, 323
- Wolfire, M. G., Hollenbach, D., & McKee, C. F. 2010, *ApJ*, 716, 1191